Photochemical & Photobiological Sciences (2023) 22:1223–1231
https://doi.org/10.1007/s43630-023-00363-y

ORIGINAL PAPERS

Photocatalytic activity of P-doped TiO_2 photocatalyst

Raffaella Rescigno[1] · Olga Sacco[1] · Vincenzo Venditto[1] · Alessandra Fusco[2] · Giovanna Donnarumma[2] · Mariateresa Lettieri[3] · Rosalba Fittipaldi[3] · Vincenzo Vaiano[4]

Received: 29 August 2022 / Accepted: 4 January 2023 / Published online: 19 January 2023

Abstract
In this study, P-doped TiO_2 photocatalysts with different molar percentages (in the range 0.071–1.25 mol %) of the non-metallic element were prepared and their photocatalytic activity under visible light irradiation was tested. All achieved samples were characterized by XRD, Raman, UV–Vis DRS and SEM–EDX techniques. XRD and Raman analysis showed that all doped photocatalysts were in anatase phase and evidenced that P ions were successfully incorporated into the TiO_2 crystal lattice, affecting also the crystallinity degree of the P-doped TiO_2 photocatalysts. Noticeably, the UV–Vis DRS spectra evidenced that the highest redshift in absorption edge was observed for the photocatalyst with the lowest P content (0.071PT), which showed also the lowest bandgap (2.9 eV). The photocatalytic performances of all P-doped TiO_2 samples were compared with that of commercial TiO_2 by evaluating the decolorization of methylene blue (MB) dye under visible light irradiation. Results showed that phosphorus doping strongly promoted photocatalytic activity in the presence of visible light. Furthermore, the most active photocatalyst in visible light tests (0.071PT) also showed better photocatalytic activity than commercial TiO_2 in the decolorization of MB under simulated sunlight irradiation. Finally, 0.071PT photocatalyst was preliminarily tested against *Escherichia coli* (*E. coli*) under simulated solar light, showing an inactivation efficiency of 90% after 2 h of treatment time.

✉ Vincenzo Venditto
vvenditto@unisa.it

✉ Giovanna Donnarumma
giovanna.donnarumma@unicampania.it

[1] Department of Chemistry and Biology, INSTM Unit, University of Salerno, Via Giovanni Paolo II, 84084 Fisciano, Salerno, Italy

[2] Department of Experimental Medicine, Section of Microbiology and Clinical Microbiology, Sant'Andrea delle Dame Complex, University of Campania "Luigi Vanvitelli", Via De Crecchio 7, 80138 Naples, Italy

[3] CNR-SPIN, c/o University of Salerno, Via Giovanni Paolo II 132, 84084 Fisciano, Salerno, Italy

[4] Department of Industrial Engineering, University of Salerno, via Giovanni Paolo II, 132, 84084 Fisciano, Salerno, Italy

Graphical abstract

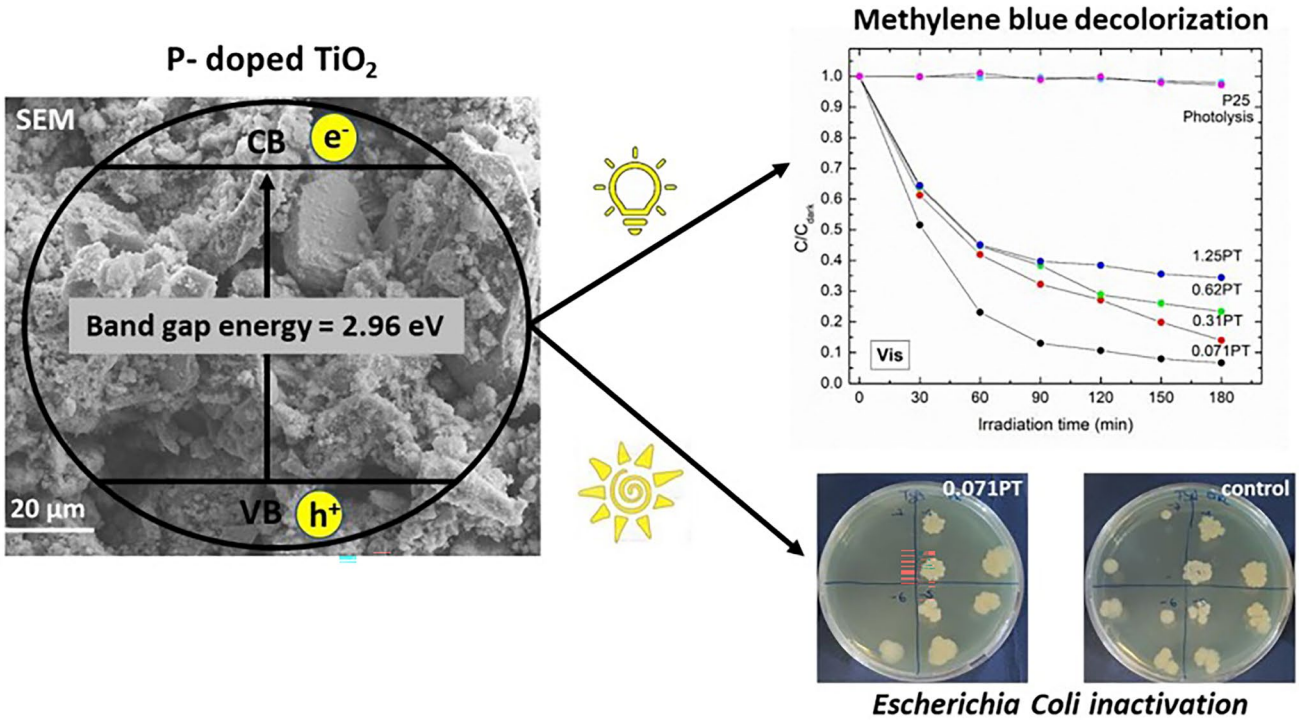

Keywords Phosphorus-doped-TiO_2 · Photocatalysis · Visible light · Solar light methylene blue · *Escherichia coli* · Antibacterial activity

1 Introduction

The sun is radiating our planet earth from billions of years, and it is the essential source of energy for life. Therefore, it is important to exploit the abundance of solar energy for a variety of applications such as energy production and environmental cleanup [1]. Among the possible approaches to convert solar energy into chemical energy, photocatalysis has become a hot research spot [2]. In fact, a photocatalytic process is able to accelerate and enhance a light-induced reaction thanks to the presence of a semiconductor, generally called "photocatalyst". Titanium dioxide is the most widely used photocatalyst material due to its properties: it is (i) economical, (ii) non-toxic, (iii) stable and highly resistant to chemicals, and, finally (v) it has a solid oxidizing power [3]. Therefore, TiO_2 photocatalysis has been found application in various fields such as air purification, self-cleaning devices, water disinfection [4], and wastewater treatment [5].

However, the bandgap energy of TiO_2, greater than 3.2 eV, makes it photocatalytically active only when irradiated by UV light. Therefore, it cannot efficiently exploit sunlight (UV radiation is only 3–5% of solar spectrum) [6].

In order to better exploit solar energy, research on photocatalytic systems based on TiO_2 anatase has focused on doping the semiconductor lattice with metallic (e.g., Fe, Cr, Pr) [7, 8] or non-metallic elements (e.g., N, P, S, C, F, or I) [9–12] able to modify the TiO_2 electronic structure and reduce the bandgap energy. Indeed, when the TiO_2 lattice is doped with metallic elements, new energy levels of energy less than that of TiO_2 conduction band are added, causing a decrease in the bandgap. When instead the TiO_2 lattice is doped with non-metallic elements, new energy levels of energy greater than that of TiO_2 valence band are added and a reduction of the bandgap energy again results [13].

Among the various non-metals, a certain interest has been directed in the last 10 years toward P as a dopant element [14]. Reported P-doped TiO_2 catalysts showed a narrower bandgap and a photocatalytic activity under UV irradiation better than both undoped TiO_2 anatase and reference Degussa P25 (TiO_2 anatase–rutile mixtures) [15]. In addition, Lin et al. [9] showed a narrow bandgap and absorption in the visible light region for P-doped TiO_2, resulting in the decolorization capacity of organic contaminants in the aforementioned electromagnetic spectrum region.

Table 1 Volume of H_3PO_4 used for P–TiO_2 preparation, nominal P/Ti molar ratio percentage, measured P/Ti molar ratio percentage (EDX), crystalline size, specific surface area and bandgap values

Samples	H_3PO_4 (µL)	Nominal P/Ti (mol %)	Measured P/Ti (mol%)	Crystallite size (nm)	Specific surface area (m^2/g)	Bandgap (eV)
TiO_2 (P25)	–		–	22	56 [27]	3.2
0.071PT	2	0.071	0.008 ± 0.003	12	84	2.9
0.31PT	8.7	0.31	0.022 ± 0.003	6	169	3.0
0.62PT	17.5	0.62	0.028 ± 0.001	6	173	3.0
1.25PT	35	1.25	0.056 ± 0.006	6	225	3.0

In this paper, the optimal P content for TiO_2 doping was investigated, using different molar percentages of the non-metallic element, in order to verify the photocatalytic activity under visible light irradiation.

All the prepared P-doped TiO_2 photocatalysts were characterized by XRD, Raman, UV–Vis DRS and SEM–EDX and the photocatalytic activity under visible light was compared with that of commercial TiO_2 (P25) in the methylene blue (MB) decolorization, chosen as a model pollutant.

The P–TiO_2 photocatalyst with the best photocatalytic activity under visible light was then used under simulated solar light to evaluate MB decolorization and antibacterial activity against *Escherichia coli.* It is important to point out that studies on the antimicrobial activity of P-doped TiO_2 under solar light have not been carried out to date.

2 Materials and methods

2.1 Materials

Titanium (IV) isopropoxide ($C_{12}H_{26}O_4Ti$, purity = 97%), and Methylene Blue ($C_{16}H_{18}ClN_3S$) were provided by Sigma Aldrich.

Phosphoric acid (H_3PO_4, purity = 85%) was provided by Honeywell Riedel-de-Haën™ (Germany).

2.2 Bacterial strain

Escherichia coli (ATCC® 43893™) was cultured in Luria–Bertani broth (Oxoid; Unipath, Basingstoke, UK) at 37 °C for 18 h. Before the experiments, the overnight culture was resuspended at 0.1 optical density (O.D.) in sterile distilled water.

2.3 Preparation of P–TiO_2 photocatalysts

Titanium (IV) isopropoxide and phosphoric acid [14] were used as precursors for TiO_2 and the dopant element, respectively.

In order to obtain P-doped TiO_2 samples at different P molar percentages, a certain volume of H_3PO_4 (85 wt%) [14] (Table 1) was added to 50 mL of distilled water and then, 12.5 mL of $C_{12}H_{26}O_4Ti$ was added dropwise to the acidified water. The whole system was kept under continuous stirring until milky colloidal suspension was obtained. The obtained suspension was centrifuged for the separation of a precipitate, which was washed three times with bi-distilled water. The recovered precipitate was then calcined in a muffle furnace for 30 min at 450 °C in static air.

The obtained photocatalysts were named xPT, where *x* is the nominal P/Ti molar ratio percentage (Table 1) and "PT" indicates the two elements: phosphorus and titanium.

2.4 Characterization techniques

The specific surface area (S_{BET}) was determined by dynamic adsorption measurements of N_2 at – 196 °C, using a Nova Quantachrome 4200e.

The X-ray (XRD) patterns were obtained with a Brucker D8 Advance diffractometer, using a nickel filtered Cu-Kα radiation and Bragg–Brentano θ–θ geometry. The 2θ acquisition interval was 5–80°, with a step size of 0.0303° and a scanning acquisition time of 0.200 s/point.

The crystallite size was calculated using the Debye–Scherrer formula (Eq. 1) considering the TiO_2 (101) crystalline plane:

$$D = \frac{K\lambda}{\beta \cos\theta} \quad (1)$$

where D is the average crystallite size (nm), K is the particle shape factor taken as 0.89, λ is the X-ray wavelength corresponding to the Cu-Kα irradiation (1.5418 Å), β is the calibrated half-intensity width of the selected diffraction peak (degrees) and θ represents the diffraction angle of TiO_2 (101) crystalline plane.

Raman spectra were obtained, at room temperature, with a dispersive MicroRaman (Invia, Renishaw) equipped with a 514 nm diode laser in the range 100–800 cm^{-1}. Diffuse reflectance spectra (UV–Vis DRS) were measured with a Perkin-Elmer Lambda 35 spectrophotometer using a RSA-PE-20 reflectance spectroscopy accessory (Labsphere Inc., North Sutton, NH). The bandgap values were then

determined using the Kubelka–Munk function (F(R∞)), by plotting $[F(R\infty)\ h\upsilon]^{0.5}$ vs hυ (eV). The surface morphology was characterized by a field emission scanning electron microscope (FESEM) (ΣIGMA, Carl Zeiss AG, Oberkochen, Germany), with a nominal resolution of 1.3 nm at 20 kV. The SEM micrographs have been acquired using an acceleration voltage of 10 kV, a working distance of 7 mm and a beam current of 80 µA. An energy dispersive X-ray (EDX) spectrometer, coupled to a scanning electron microscope (SEM) (LEO Evo 50, Carl Zeiss AG, Oberkochen, Germany), was employed to determine the elemental composition of the photocatalyst powders. The analysis was performed using Oxford Inca software; electron beam of energy of 20 keV and probe current of about 350 pA were applied. P/Ti ratio was calculated using atomic percentage of the elements measured by EDX analyses in various areas with size of $275 \times 200\ \mu m^2$.

2.5 Photocatalytic activity tests under visible light

The photocatalytic tests in the presence of visible light were carried out using a Pyrex cylindrical reactor (ID = 3.5 cm, $h = 28$ cm, $V = 269$ mL). The irradiation was performed with four Vis lamps (Philips, nominal power: 8 W, with emission in the range 400–750 nm) or four solar lamps (Krypton-Argon lamps, SUN-GLO 8 W T5, nominal power: 8 W) placed at 10 cm from the external surface of the reactor. The P–TiO_2, in form of powder (225 mg), was added to 75 mL of aqueous solution at 5 mg/L of MB. Before starting the irradiation, the suspension was maintained in dark conditions for 30 min to achieve the adsorption/desorption equilibrium of MB on the catalyst surface (MB concentration at equilibrium was referred to as C_{dark}) and then the lamps were turned on for a time equal to 180 min.

A volume (1.5 mL) of suspension was withdrawn from the photoreactor at increasing times during irradiation and centrifuged to get the solutions for the analysis of the residual MB dye concentration. A Duetta fluorescence spectrometer (Horiba Scientific) was used to measure the MB absorbance at 663 nm.

2.6 Antibacterial activity tests under simulated solar light

Antibacterial activity was tested using simulated solar light by three 8 W Krypton-Argon lamps (SUN-GLO 8 W T5) placed at about 5 cm from the external surface of the test tube containing 5 ml of 0.1 O.D. of water suspension of *E. coli* in the presence of 3 mg/ml powder photocatalyst. The tubes were placed on a magnetic stirrer and exposed to solar light for 2 h at room temperature in constant agitation to facilitate the powder resuspension. As a positive control, a sample of bacterial suspension incubated at room temperature for 2 h without light and P–TiO_2 powder was used. At the end of this time, bacterial suspension was serial diluted (that is diluting it 1:10 serially, taking 100 µl and adding them to 900 µl of water) and plated on Luria–Bertani agar (OXOID) and incubated at 37 °C overnight to quantify viable intracellular bacteria (CFUs /ml).

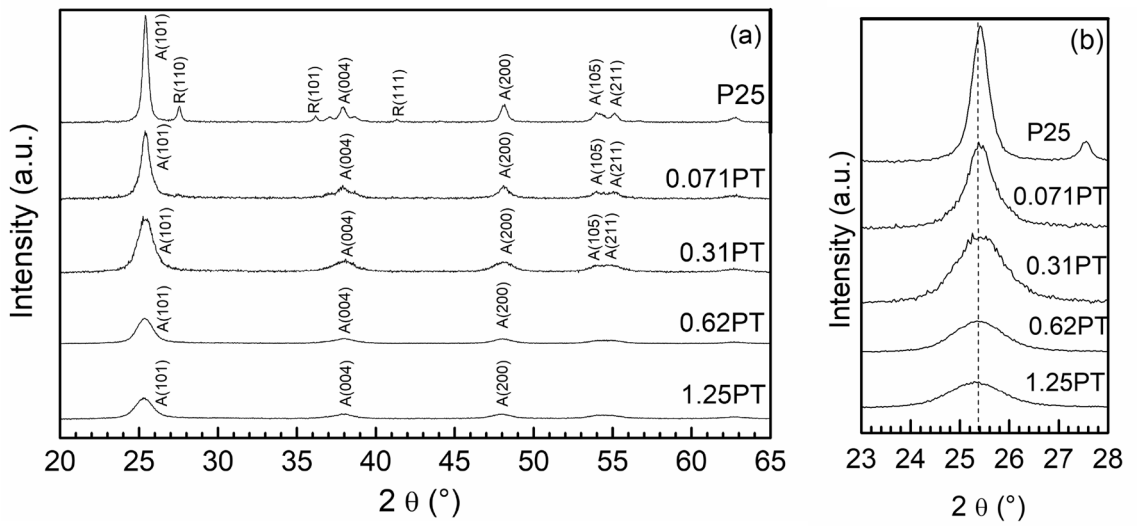

Fig. 1 X-ray diffraction patterns of 0.071PT, 0.31PT, 0.62PT, 1.25PT and commercial TiO_2 (P25); *A* anatase; *R* rutile: **a** in the range 20–65° and **b** in the range 23–28°

3 Results and discussion

3.1 Characterization results

XRD spectra of all P–TiO_2 samples are compared in Fig. 1 with that of a commercial TiO_2 sample (Degussa P25). As expected, in the XRD pattern of P25, TiO_2 anatase-phase reflections (101), (004), (200), (105), and (211), at 2θ 25.4, 37.9, 48.02, 53.9, and 55.4°, respectively (ICDD No. 21–1272) and TiO_2 rutile-phase reflections (110), (101) and (111), at 2θ 27.50, 36.05 and 41.22°, respectively (ICDD No. 21–1276) [16], are both present. On the other hand, P–TiO_2 samples showed the typical diffraction patterns of TiO_2 anatase phase (Fig. 1a). Furthermore, no segregated phases (i.e., phosphorus oxides) were observed, thus indicating that the phosphorus could be effectively incorporated into the host semiconductor lattice [17]. A careful analysis of XRD spectra of all photocatalysts in the 2θ range between 23 and 28° (Fig. 1b) highlights a shift of the (101) peak toward lower diffraction angles, greater for higher phosphorus contents, confirming the phosphorus inclusion into TiO_2 lattice. Moreover, the entity of this observed shift for P-doped TiO_2 samples is similar to that reported in scientific papers dealing with the doping of TiO_2 with phosphorus and it is an evidence of the formation of an interstitial P/TiO_2 solid solution [18–20].

Nevertheless, with the increase of P content, average crystallite sizes (Table 1), calculated with the Debye–Scherrer equation (Eq. 1), of P–TiO_2 samples decrease from 12 to almost 6 nm, which corresponds, as commonly accepted, to an increase of crystalline surface and defects and, as a consequence, to a decrease of crystallinity [21]. This behavior suggests that the incorporation of even small amounts of phosphorus greatly influences the crystallization process by reducing the crystallinity degree of the doped samples [22, 23].

Raman spectra are presented in Figure S1 of Supplementary Material. All the P–TiO_2 photocatalysts display Raman bands located at about 141 cm^{-1} (Eg), 199 cm^{-1} (Eg), 398 cm^{-1} (B1g), 513 cm^{-1} (A1g) and 639 cm^{-1} (Eg), assigned to anatase TiO_2 [24], confirming that all P-doped TiO_2 samples are in the such crystalline phase, as also evidenced by XRD results. Noticeably, the intensity reduction of all the Raman signals and their enlargement, as the phosphorus content increases, is clearly evident. This phenomenon, related to the increase in phosphorus content, could be ascribed to the decrease in crystallite size (Table 1) or even to the progressive symmetry destruction of the Ti–O–Ti lattice (a similar result was observed in iodine-doped TiO_2) [10]. It is worthwhile to note that, consistently with the available literature [24], the progressive decrease of Raman signals with the increase of P content excludes the possible presence of PO_4^{3-} bonded on the surface of all P-doped samples.

Figure 2 reports the Tauc plot for the optical indirect bandgap evaluation of all P-doped samples and TiO_2 (P25) (Figure S2 of Supplementary Material for the curves in the range 1.5–4 eV). The data evidenced that the absorption edge of pure TiO_2 (P25) is located at about 3.2 eV (corresponding to about 385 nm) [25], whereas for 0.31PT, 0.62PT and 1.25PT samples, it moves to about 3.0 eV (corresponding to about 410 nm). The highest redshift in absorption edge is observed for 0.071PT, being located at about 2.9 eV (corresponding to about 425 nm).

The calculated bandgap values (E_{bg}) of P-doped samples were summarized in Table 1. Referring to the available literature, the bandgap energy decrease, observed in the doped samples, is possibly due to the replacement of phosphorus ions to Ti^{4+} which leads to a slight rise of

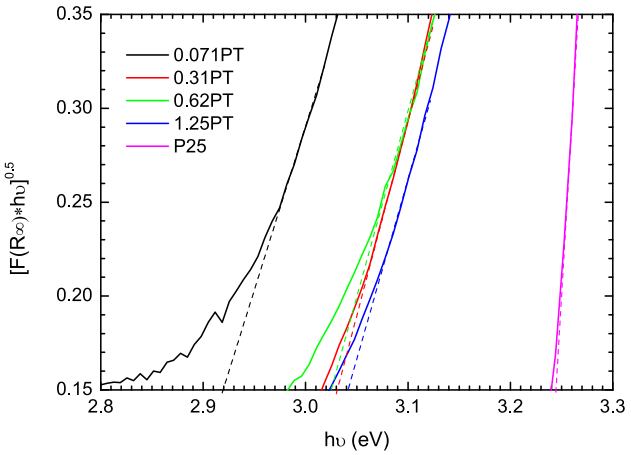

Fig. 2 Tauc plot for the optical indirect bandgap energy calculus of 0.071PT, 0.31PT, 0.31PT, 1.25PT and TiO_2 (P25)

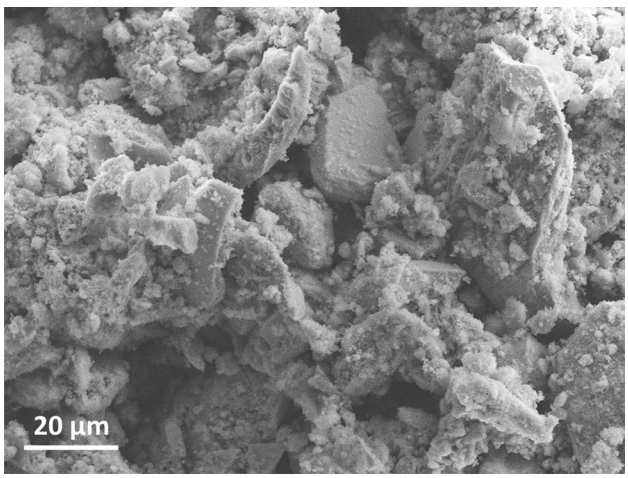

Fig. 3 SEM image of the 0.31PT sample

the valence band energy position and a narrowing of the bandgap value [23, 26].

The specific surface area (S_{BET}) of all the photocatalysts is shown in Table 1. For all doped samples, S_{BET} increases by increasing the P content. These data agree with the XRD results, which evidenced that the doping with phosphorus inhibits the growth of P–TiO_2 crystals and, in the absence of crystallites aggregation phenomena, determines a significant increase in the surface area.

SEM observations showed that, irrespective of the P content, the powder photocatalyst samples consisted of particles having different appearance, sizes and shapes. Small and large porous aggregates, exhibiting sponge-like structure, and irregular flakes, with flat faces and edges, were recognized in all the samples. In Fig. 3, micrograph of the sample 0.31PT is reported as a representative example of the morphology of the powder P–TiO_2 samples.

EDX analysis, performed on the powder P–TiO_2 samples, verified the presence of Ti, O, and P as elements. The measured P/Ti ratios are reported in Table 1. In the investigated P/Ti ratio range, the experimental and nominal P content have a linear trend. However, in all samples, a lower experimental P/Ti value than the nominal one was found; the difference between the measured and expected composition was greater in the samples with higher amounts of dopant. Similar behavior has been reported for other doped TiO_2 powders [28, 29]. It is to point out that P, Ti and O elements and comparable composition were found by EDX analysis in different morphological structures (i.e., porous aggregates and flat flakes) of the same sample.

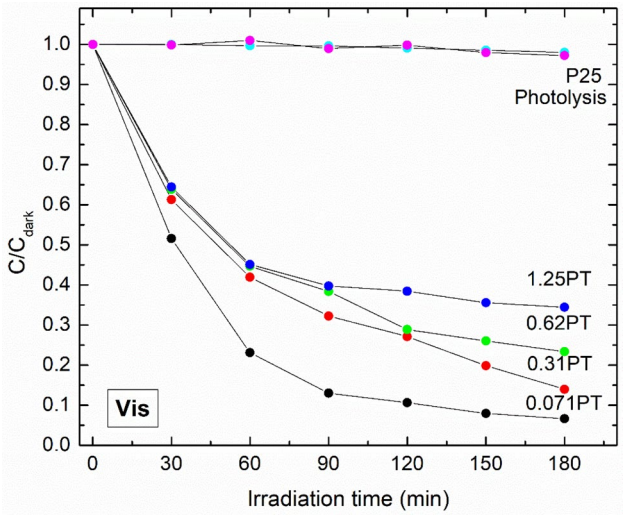

Fig. 4 Photocatalytic decolorization of MB by different P–TiO_2 powder photocatalysts under visible light irradiation

3.2 Photocatalytic activity results under visible light

The photocatalytic activity of commercial TiO_2 (P25) and P–TiO_2 powder samples was assessed in the MB decolorization under visible light (Fig. 4). A control test (without the photocatalyst), carried out to verify the photolysis contribution to decolorization, showed that the MB relative concentration did not significantly change during the overall irradiation time. On the other hand, an evident decrease of MB relative concentration resulted using the P–TiO_2 photocatalysts, underlining that the doping with phosphorous promotes the photocatalytic activity in the presence of visible light. The observed absence of any MB decolorization in the presence of TiO_2 P25 allows to exclude possible photosensitization phenomena of TiO_2 surface by the dye molecules. As regards the influence of P content, the photocatalyst with the lowest P content (0.071PT) showed the highest photocatalytic efficiency compared with the other P–TiO_2 samples, leading to an MB decolorization of 97% after 180 min of light irradiation.

To further verify the influence of P loading on photocatalytic activity, the pseudo-first-order rate kinetic constant (k) for MB photocatalytic decolourization was calculated [30, 31]. The k values were evaluated by the slope of the straight line obtained by plotting $-ln\left(\frac{C}{C_0}\right)$ vs the irradiation time (t) according to the following equation (Eq. 2):

$$-ln\left(\frac{C}{C_0}\right) = k \bullet t \tag{2}$$

where C is the concentration of MB (mg L^{-1}); C_0 is the concentration of MB after dark period (mg L^{-1}); k is the pseudo-first-order rate kinetic constant (min^{-1}).

The kinetic constant values are reported in Figure S3 of Supplementary Material.

The overall rate constants for MB decolorization were found to be in the following order: $k_{0.071PT} > k_{0.31PT} > k_{0.62PT} > k_{1.25PT}$.

These results are essentially in agreement with the E_{bg} values reported in Table 1, which indicate that 0.071PT photocatalyst, having the lowest E_{bg} value (2.9 eV), exhibited the fastest decolorization kinetic under visible light. On the other hand, the lower photocatalytic activity observed for 0.31PT, 0.62PT and 1.25PT photocatalysts can be explained by considering that, for such photocatalysts, the crystalline size and crystallinity degree is lower than 0.071PT sample (as evidenced from XRD and Raman results). Both these structural parameters are critical for the photocatalytic performance of TiO_2 [32] and it is commonly accepted that the photo-reactivity is enhanced by increasing the crystallinity [33, 34].

It is worth noting that the S_{BET} values of P-doped TiO_2 photocatalysts have an opposite trend to that of kinetic constant values, as S_{BET} increases with the increase of P content.

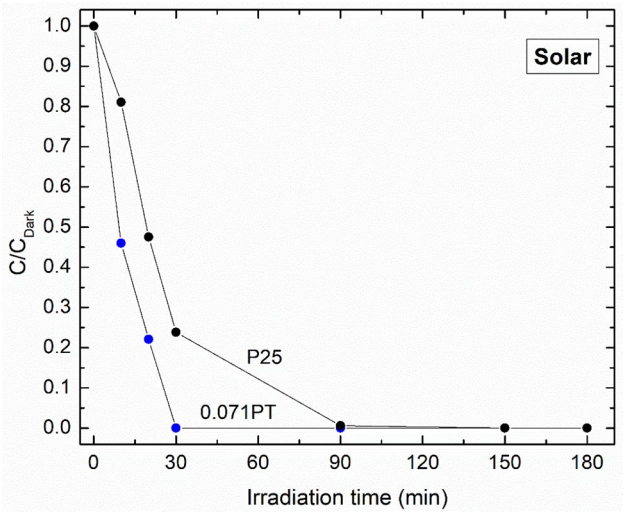

Fig. 5 Photocatalytic decolorization of MB by 0.071PT and TiO_2 P25 photocatalyst powder samples under simulated solar light irradiation

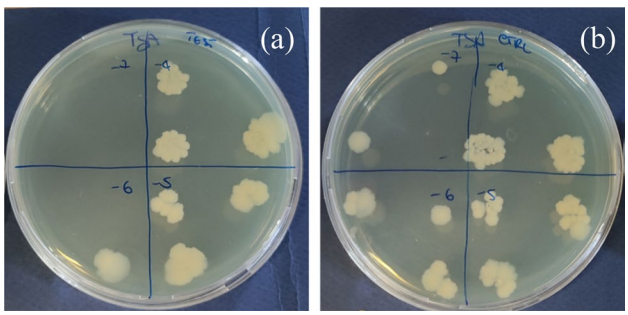

Fig. 6 Picture of *E.coli* colonies: **a** after photocatalytic treatment with 0.071PT; **b** control test

Based on these observations, we can argue that the main reasons for 0.071PT photocatalyst high activity under visible light irradiation are the observed red shift in the absorption edge as well as the little influence exerted by the low amount of phosphorus included into the TiO_2 lattice on the photocatalyst crystallinity. Such behavior well agrees with previous papers dealing with the study P-doped TiO_2 photoactivity under visible light [14, 23].

The photocatalytic performances of the best sample (0.071PT) were compared with different data from some papers dealing with the preparation of P-doped TiO_2 and studied for the photocatalytic decolorization of MB dye (Table S1 of Supplementary Material). The data reported in Table S1 confirmed the very interesting photocatalytic performances of the 0.071PT sample prepared in this paper compared to Jin et al. [23], Zheng et al. [35] and Gopal et al. [14]. Although the kinetics reported by Niu et al. [36] are faster, the light source power (500 W halogen–tungsten lamp) used by them was higher than that used in the present paper (four 8 W Vis lamps). Furthermore, it is worthwhile to note that, conversely to our work, such authors doped TiO_2 with P content significantly higher than that of 0.071PT photocatalyst, evidencing that the preparation procedure adopted in this work allows to formulate an effective visible light active photocatalyst using a very low P content for TiO_2 doping, thus making the photocatalyst more sustainable from an environmental point of view.

3.3 Results of MB decolorization and antibacterial inactivation under simulated solar light

The P–TiO_2 photocatalyst most active in MB decolorization under visible light (0.071 PT) was then used to evaluate MB decolorization and *Escherichia coli* inactivation, under simulated solar light irradiation.

The photocatalytic activity of P25 and 0.071PT samples in the MB decolorization under simulated solar light is reported in Fig. 5.

The decrease rate of MB relative concentration using 0.071PT photocatalyst is higher than P25, underlining that the doping with phosphorous is able to improve the photocatalytic activity also in presence of simulated solar light, achieving better performance than commercial TiO_2.

The antibacterial activity tests under simulated solar light evidenced that 0.071PT photocatalyst can reduce also bacterial growth (Fig. 6). In fact, in the control sample, a bacterial concentration of 10 [8] CFUs/mL was found, whereas in the presence of the 0.071PT photocatalyst, the *E. coli* concentration lowers to about 10 [7] CFUs/mL (90% inactivation), after 2 h of treatment time.

As the latter is only a preliminary test, further study is necessary to optimize the operating conditions (i.e., 0.071PT dosage and pH of the *E. coli* aqueous solution) in order to achieve better performances under simulated solar light.

4 Conclusions

In this work, TiO_2 was doped with P at different nominal P/Ti molar ratio percentages (in the range of 0.071–1.25 mol %). XRD and Raman analysis results showed that all the achieved P–TiO_2 samples were in the anatase phase, evidencing that the crystallinity degree decreased with increasing the P content. The UV–Vis DRS characterization showed that all doped catalysts present a redshift in absorption edge and bandgap values were in the range of 2.9–3.0 eV. This behavior is associated to the presence of P ions in the TiO_2 lattice, as detected by the shift of the (101) reflection of TiO_2 in the XRD spectrum. SEM–EDX analyses confirmed the presence of P with a P/Ti ratio in the range of 0.008–0.056 mol%.

The photocatalytic performance of all samples was evaluated by analyzing the methylene blue (MB) dye decolorization under visible light irradiation. The sample 0.071PT, having the lowest P content (P/Ti = 0.008 mol%), showed the highest photocatalytic efficiency, leading to a 97% decolorization of MB after 180 min of light irradiation. The 0.071PT photocatalyst was also tested under simulated solar light irradiation to evaluate MB decolorization and antibacterial activity against *E. coli.* The experimental results evidenced that 0.071PT allowed to achieve the total MB decolorization after 30 min of irradiation and *E. coli* inactivation efficiency of 90% after 2 h of treatment time.

Supplementary Information The online version contains supplementary material available at https://doi.org/10.1007/s43630-023-00363-y.

Funding Open access funding provided by Università degli Studi di Salerno within the CRUI-CARE Agreement.

Declarations

Conflict of interest On behalf of all the authors, the corresponding author states that there is no conflict of interest.

References

1. Lee, J., & Gouma, P. I. (2012). Sol-Gel processed oxide photocatalysts. In M. Aparicio, A. Jitianu, & L. C. Klein (Eds.), *Sol-Gel processing for conventional and alternative energy* (pp. 217–237). Boston, MA: Springer US. https://doi.org/10.1007/978-1-4614-1957-0_11
2. Meng, X.; Eluagwule, B.; Wang, M.; Wang, L.; Zhang, J. 2020 Solar photocatalysis for environmental remediation. In handbook of smart photocatalytic materials. Elsevier, pp 183–195. https://doi.org/10.1016/B978-0-12-819049-4.00013-1
3. Schneider, J., Matsuoka, M., Takeuchi, M., Zhang, J., Horiuchi, Y., Anpo, M., & Bahnemann, D. W. (2014). Understanding TiO $_2$ photocatalysis: mechanisms and materials. *Chemical Reviews, 114*(19), 9919–9986. https://doi.org/10.1021/cr5001892
4. Yadav, H. M., Kim, J.-S., & Pawar, S. H. (2016). Developments in photocatalytic antibacterial activity of nano TiO2: A review. *Korean Journal of Chemical Engineering, 33*(7), 1989–1998. https://doi.org/10.1007/s11814-016-0118-2
5. Pelaez, M., Nolan, N. T., Pillai, S. C., Seery, M. K., Falaras, P., Kontos, A. G., Dunlop, P. S. M., Hamilton, J. W. J., Byrne, J. A., O'Shea, K., Entezari, M. H., & Dionysiou, D. D. (2012). A review on the visible light active titanium dioxide photocatalysts for environmental applications. *Applied Catalysis B: Environmental, 125*, 331–349. https://doi.org/10.1016/j.apcatb.2012.05.036
6. Ohtani, B. (2013). Titania photocatalysis beyond recombination: A critical review. *Catalysts, 3*(4), 942–953. https://doi.org/10.3390/catal3040942
7. Peng, Y.-H., Huang, G.-F., & Huang, W.-Q. (2012). Visible-light absorption and photocatalytic activity of Cr-Doped TiO2 nanocrystal films. *Advanced Powder Technology, 23*(1), 8–12. https://doi.org/10.1016/j.apt.2010.11.006
8. Mancuso, A., Sacco, O., Vaiano, V., Sannino, D., Pragliola, S., Venditto, V., & Morante, N. (2021). Visible light active Fe-Pr Co-doped TiO2 for water pollutants degradation. *Catalysis Today, 380*, 93–104. https://doi.org/10.1016/j.cattod.2021.04.018
9. Lin, L., Lin, W., Zhu, Y., Zhao, B., & Xie, Y. (2005). Phosphor-doped titania —a novel photocatalyst active in visible light. *Chemistry Letters, 34*(3), 284–285. https://doi.org/10.1246/cl.2005.284
10. Liu, G., Chen, Z., Dong, C., Zhao, Y., Li, F., Lu, G. Q., & Cheng, H.-M. (2006). Visible light photocatalyst: Iodine-doped mesoporous titania with a bicrystalline framework. *The Journal of Physical Chemistry B, 110*(42), 20823–20828. https://doi.org/10.1021/jp062946m
11. Yu, W., Liu, X., Pan, L., Li, J., Liu, J., Zhang, J., Li, P., Chen, C., & Sun, Z. (2014). Enhanced visible light photocatalytic degradation of methylene Blue by F-doped TiO2. *Applied Surface Science, 319*, 107–112. https://doi.org/10.1016/j.apsusc.2014.07.038
12. Piątkowska, A., Janus, M., Szymański, K., & Mozia, S. (2021). C-, N- and S-doped TiO2 photocatalysts: A review. *Catalysts, 11*(1), 144. https://doi.org/10.3390/catal11010144
13. Patil, S. B., Basavarajappa, P. S., Ganganagappa, N., Jyothi, M. S., Raghu, A. V., & Reddy, K. R. (2019). Recent advances in non-metals-doped TiO2 nanostructured photocatalysts for visible-light driven hydrogen production, CO2 reduction and air purification. *International Journal of Hydrogen Energy, 44*(26), 13022–13039. https://doi.org/10.1016/j.ijhydene.2019.03.164
14. Gopal, N. O., Lo, H.-H., Ke, T.-F., Lee, C.-H., Chou, C.-C., Wu, J.-D., Sheu, S.-C., & Ke, S.-C. (2012). Visible light active phosphorus-doped TiO $_2$ nanoparticles: An EPR evidence for the enhanced charge separation. *Journal of Physical Chemistry C, 116*(30), 16191–16197. https://doi.org/10.1021/jp212346f
15. Yu, J. C., Zhang, L., Zheng, Z., & Zhao, J. (2003). Synthesis and characterization of phosphated mesoporous titanium dioxide with high photocatalytic activity. *Chemistry of Materials, 15*(11), 2280–2286. https://doi.org/10.1021/cm0340781
16. Zouzelka, R., & Rathousky, J. (2017). Photocatalytic abatement of NOx pollutants in the air using commercial functional coating with porous morphology. *Applied Catalysis B: Environmental, 217*, 466–476. https://doi.org/10.1016/j.apcatb.2017.06.009
17. Dosa, M., Piumetti, M., Bensaid, S., Andana, T., Galletti, C., Fino, D., & Russo, N. (2019). Photocatalytic abatement of volatile organic compounds by TiO_2 nanoparticles doped with either phosphorous or zirconium. *Materials, 12*(13), 2121. https://doi.org/10.3390/ma12132121
18. Ansari, S. A., & Cho, M. H. (2016). Highly visible light responsive, narrow band gap TiO_2 nanoparticles modified by elemental red phosphorus for photocatalysis and photoelectrochemical applications. *Science and Reports, 6*(1), 25405. https://doi.org/10.1038/srep25405
19. Yu, H.-F. (2007). Photocatalytic abilities of gel-derived P-doped TiO_2. *Journal of Physics and Chemistry of Solids, 68*(4), 600–607. https://doi.org/10.1016/j.jpcs.2007.01.050
20. Mendiola-Alvarez, S. Y., Aracely Hernández-Ramírez, M., Guzmán-Mar, J. L., Garza-Tovar, L. L., & Hinojosa-Reyes, L. (2019). Phosphorous-doped TiO2 nanoparticles: synthesis, characterization, and visible photocatalytic evaluation

on sulfamethazine degradation. *Environmental Science Pollution Research, 26*(5), 4180–4191. https://doi.org/10.1007/s11356-018-2314-6

21. Dutta, D. P., & Raval, P. (2018). Effect of transition metal ion (Cr^{3+}, Mn^{2+} and Cu^{2+}) doping on the photocatalytic properties of $ZnWO_4$ Nanoparticles. *Journal Photochemistry Photobiology Chemistry, 357*, 193–200. https://doi.org/10.1016/j.jphotochem.2018.02.026
22. Mohamed, R. M., & Aazam, E. (2013). Synthesis and characterization of P-Doped TiO_2 thin-films for photocatalytic degradation of butyl benzyl phthalate under visible-light irradiation. *Chinese Journal of Catalysis, 34*(6), 1267–1273. https://doi.org/10.1016/S1872-2067(12)60572-5
23. Jin, C., Zheng, R. Y., Guo, Y., Xie, J. L., Zhu, Y. X., & Xie, Y. C. (2009). Hydrothermal synthesis and characterization of phosphorous-doped TiO_2 with high photocatalytic activity for methylene blue degradation. *Journal of Molecular Catalalysis A Chemical, 313*(1–2), 44–48. https://doi.org/10.1016/j.molcata.2009.07.021
24. Huang, R., Zhang, S., Ding, J., Meng, Y., Zhong, Q., Kong, D., & Gu, C. (2019). Effect of adsorption properties of phosphorus-doped TiO2 nanotubes on photocatalytic NO removal. *Journal of Colloid and Interface Science, 553*, 647–654. https://doi.org/10.1016/j.jcis.2019.06.063
25. Lv, Y., Yu, L., Huang, H., Liu, H., & Feng, Y. (2009). Preparation, characterization of P-doped TiO_2 nanoparticles and their excellent photocatalystic properties under the solar light irradiation. *Journal of Alloys and Compounds, 488*(1), 314–319. https://doi.org/10.1016/j.jallcom.2009.08.116
26. Yang, K., Dai, Y., & Huang, B. (2007). Understanding photocatalytic activity of S- and P-doped TiO_2 under visible light from first-principles. *Journal of Physical Chemistry C, 111*(51), 18985–18994. https://doi.org/10.1021/jp0756350
27. Raj, K. J. A., Viswanathan, B. (2009) Effect of Surface Area, Pore Volume and Particle Size of P25 Titania on the Phase Transformation of Anatase to Rutile. Indian J Chem 5
28. Zaleska, A. (2008). Doped-TiO_2: A review. *Recent Patents Engineering, 2*(3), 157–164. https://doi.org/10.2174/187221208786306289
29. Zeng, J.-B., Li, K.-A., & Du, A.-K. (2015). Compatibilization strategies in poly(Lactic Acid)-based blends. *RSC Advances, 5*(41), 32546–32565. https://doi.org/10.1039/C5RA01655J
30. Yogi, C., Kojima, K., Takai, T., & Wada, N. (2009). Photocatalytic degradation of methylene blue by Au-deposited TiO_2 film under UV irradiation. *Journal of Materials Science, 44*(3), 821–827. https://doi.org/10.1007/s10853-008-3151-7
31. Rauf, M. A., Meetani, M. A., Khaleel, A., & Ahmed, A. (2010). Photocatalytic degradation of methylene blue using a mixed catalyst and product analysis by LC/MS. *Chemical Engineering Journal, 157*(2–3), 373–378. https://doi.org/10.1016/j.cej.2009.11.017
32. Wang, X., Sø, L., Su, R., Wendt, S., Hald, P., Mamakhel, A., Yang, C., Huang, Y., Iversen, B. B., & Besenbacher, F. (2014). The influence of crystallite size and crystallinity of anatase nanoparticles on the photo-degradation of phenol. *Journal of Catalysis, 310*, 100–108. https://doi.org/10.1016/j.jcat.2013.04.022
33. Puddu, V., Choi, H., Dionysiou, D. D., & Puma, G. L. (2010). TiO_2 Photocatalyst for indoor air remediation: influence of crystallinity, crystal phase, and UV radiation intensity on trichloroethylene degradation. *Applied Catalysis B: Environmental, 94*(3–4), 211–218. https://doi.org/10.1016/j.apcatb.2009.08.003
34. Ohtani, B., Ogawa, Y., & Nishimoto, S. (1997). Photocatalytic activity of amorphous−anatase mixture of titanium(IV) oxide particles suspended in aqueous solutions. *The Journal of Physical Chemistry B, 101*(19), 3746–3752. https://doi.org/10.1021/jp962702+
35. Zheng, R., Lin, L., Xie, J., Zhu, Y., & Xie, Y. (2008). State of doped phosphorus and its influence on the physicochemical and photocatalytic properties of P-doped titania. *Journal of Physical Chemistry C, 112*(39), 15502–15509. https://doi.org/10.1021/jp806121m
36. Niu, J., Lu, P., Kang, M., Deng, K., Yao, B., Yu, X., & Zhang, Q. (2014). P-Doped TiO_2 with superior visible-light activity prepared by rapid microwave hydrothermal method. *Applied Surface Science, 319*, 99–106. https://doi.org/10.1016/j.apsusc.2014.07.048